Theoretical Study on the Mechanism of Low-Energy Dissociative Electron Attachment for Uracil†

Toshiyuki Takayanagi,* Tomoko Asakura, and Haruki Motegi

Department of Chemistry, Saitama University, 255 Shimo-Okubo, Sakura-ku, Saitama City, Saitama 338-8570, Japan

Received: October 7, 2008; Revised Manuscript Received: November 9, 2008

The lowest electronically adiabatic potential energy surface of the uracil anion has been theoretically investigated with density-functional theory methods in order to understand the mechanism of the N−H bond dissociation induced by low-energy electron attachment. We found that the BH&HLYP level can reasonably describe both the dipole-bound and valence anionic states in a balanced way. With this density-functional theory level, we have constructed two-dimensional potential energy surfaces as a function of appropriate internal coordinates and discuss the importance of electronic coupling between the dipole-bound and valence anion states in dissociative electron attachment of uracil. The transition state geometry for the electronic isomerization between the dipole-bound anion and the π^* valence anion was successfully optimized and the barrier height for this isomerization was found to be relatively low. It was found that the out-of-plane motion of H at the C_6 position plays the most important role in this isomerization process. Reduced-dimensionality quantum wave packet calculations taking two active internal coordinates into account have also been performed to interpret the resonance structures observed in cross sections for the N−H dissociation channel at a qualitative level.

1. Introduction

Since the observation that low-energy electrons cause significant DNA/RNA damage including strand breaks,[1−3] a large number of studies have been carried out for electron collisions with isolated nucleic acid base molecules in the gas phase. Previous electron−molecule scattering experimental studies revealed that low-energy electrons effectively induce fragmentation of isolated DNA/RNA pyrimidine and purine bases through dissociative electron attachment mechanisms.[4−17] It is now established that the most abundant fragment anion formed at collision energies below 3 eV is the closed shell dehydrogenated molecular anion via $e^- + M \rightarrow M^{-*} \rightarrow (M-H)^- + H$, where M stands for the parent nucleic acid base molecule and M^{-*} is the transient negative ion. Notice that this behavior simply comes from the fact that the dehydrogenated radical (M−H) has relatively large electron affinity. These gas-phase experiments have given clear evidence that low-energy electrons can cause DNA/RNA damage through bond dissociation.

Interestingly, in recent electron-scattering studies with an improved collision energy resolution, several narrow resonance peaks have been observed in dissociative electron attachment cross sections of the $(M-H)^- + H$ production channel at low collision energies below 2 eV for uracil (U) and thymine (T).[6−10,14] One report suggests that the observed resonance peaks are presumably due to the formation of different $(M-H)^-$ isomers since hydrogen atom loss can occur from several different sites.[8] However, all other recent papers conclude that those peaks can be assigned to vibrational Feshbach resonances arising from coupling between the dipole-bound state, where an excess electron is bound by the strong dipole field, and the valence anion state associated with occupation of the lowest N_1-H σ^* orbital. This means that the main two resonance peaks can be identified as the $v = 2$ and 3 vibrational levels of the N_1-H stretching mode (v is the corresponding vibrational quantum number), which should lie in energy above the $(M-H)^- + H$ dissociation threshold.[7] Other resonance peaks observed were tentatively assigned as the combination of the N_1-H stretching mode and other vibrational mode such as the C−H or C−N stretching mode.[14]

Extensive electronic structure studies have been reported for understanding the mechanism of the dissociative electron attachment processes of uracil, thymine, and other related molecules.[18−42] For example, Li et al.[26] have theoretically characterized one-dimensional potential energy curves for U^- along the N−H and C−H bonds using hybrid density-functional theory (DFT) calculations at the B3LYP level as well as the complete-basis-set approach. Although they were able to obtain reliable N−H and C−H bond dissociation energies, they noticed that the B3LYP calculations cannot describe the dipole-bound anion state at all and significantly overestimate the stability of the π^* valence anion state, where an excess electron is trapped in the π^* orbital of uracil. Scheer et al.[29] have constructed a one-dimensional potential energy curve along the N_1-H stretch coordinate with the Hartree−Fock-based configuration interaction method in order to understand the resonance contribution to the dissociative electron attachment of uracil. They have identified reasonable resonance peaks by computing Franck−Condon factors; however, the π^* valence anion state was completely ignored in their calculation. Sommerfeld[28] investigated electronic interaction between the dipole-bound anion state and π^* valence anion state of uracil using a sophisticated ab initio electronic structure method. He has found a potential energy barrier (∼0.1 eV) formed by an avoided crossing between the dipole-bound and π^* valence anionic states. Although he did not consider U^- dissociation processes, his study clearly showed that the dipole-bound state can be a doorway in dissociative electron attachment since an excess electron can be transferred from a diffuse dipole-bound orbital

† Part of the "George C. Schatz Festschrift".

* Author to whom correspondence should be addressed. Fax: +81-48-858-3700. E-mail: tako@mail.saitama-u.ac.jp.

10.1021/jp808885x CCC: $40.75
Published on Web 12/09/2008

into a compact π^* valence orbital to form a long-lived anion. Very recently, large-scale ab initio electronic structure calculations using extrapolation schemes have been carried out to obtain accurate energy levels of the π^* valence anion states for uracil and thymine.[30,31,36,42] These studies show that the π^* valence anion state for uracil is slightly more stable than the neutral state after zero-point vibrational energy corrections.

In this paper we discuss in more detail the dissociative electron attachment process of uracil, $e^- + U \rightarrow U^{-*} \rightarrow (U-H)^- + H$, from a theoretical viewpoint. As mentioned above, only Scheer et al.[29] are proposing a dissociation mechanism through the coupling of the diffuse dipole-bound state and the low-lying σ^* anionic state. They succeeded qualitatively in interpreting the observed resonance structure with a simple one-dimensional potential energy model; however, their treatment is too simple since only the N_1-H stretching coordinate is taken into account in the dynamics. In particular, it should be important to investigate the importance of the π^* valence anionic state in the dissociation process, as Sommerfeld has previously suggested.[28,43−45] Here we extend the theoretical work of Scheer et al. to include another active coordinate in the dynamics so as to describe the dipole-bound state and π^* and σ^* valence anionic states simultaneously. We believe that the present theoretical study would be a good starting point for further quantitative interpretations of the observed resonance structures.

2. Choice of an Appropriate DFT Level for Uracil Anion

As mentioned before, uracil can form two different types of bound-electron anion states: the diffuse dipole-bound state, where an extra electron is attached to the electrostatic dipole attractive potential, and valence anion state, where an excess electron occupies a compact valence orbital. Therefore, equilibrium geometries for these two states are consequently very different; the dipole-bound anion geometry is very close to the neutral minimum structure with planar C_s symmetry, while the π^* valence anion state has a puckered ring structure with C_1 symmetry. Since these two anion states have very different electronic structures, different computational approaches have been traditionally employed to characterize the energetics and structures of these anions. However, in order to understand the mechanism of the dissociative electron attachment process and to obtain a global feature of the anion potential energy surface, one has to employ an appropriate computational level that can describe both anion states in a balanced way. In this work we employ DFT methods although most of the previous theoretical studies based on DFT calculations failed to describe both anion states simultaneously. Nevertheless, since DFT calculations are computationally less expensive and geometry optimization schemes using analytical first derivatives can easily be applied, the DFT methods are suitable for obtaining global pictures of potential energy surfaces. In addition, it may be important to know which DFT method can describe both anion states since various exchange-correlation functionals have been proposed so far.

First, we have carried out geometry optimization for both the dipole-bound anion and valence anion states of uracil using various DFT methods with the 6-311++G(2d,p) basis set. For hydrogen atoms, we have further added two diffuse sp functions whose exponents of the s functions are 0.012 and 0.04 while those of the p functions are 0.25 and 0.0833. These exponents were obtained from the outermost sp functions of the 6-311++G(2d,p) basis set by using a scaling factor of 3. We have examined a total of 5 DFT methods: B3LYP,[46,47] BH&H,[47−49] BH&HLYP,[47−49] B3PW91,[46,50] and X3LYP[51] implemented in the GAUSSIAN-03 code.[52] The potential energy profiles were then calculated along the straight line vector connecting the two minimum geometries with

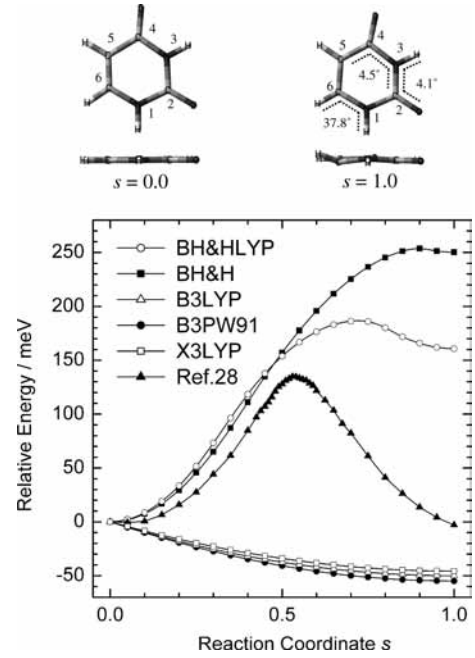

Figure 1. Potential energy profiles of uracil anion along the linear scaling factor s calculated with several DFT levels of theory; $s = 0$ and 1 correspond to the geometries of the diffuse dipole-bound and valence anion states, respectively. Filled triangles represent the ab initio ADC result of Sommerfeld taken from ref 28. Structures for dipole-bound and valence anions optimized at the BH&HLYP level are also shown.

$$x(s) = x^{DBA} - s(x^{DBA} - x^{VA}) \quad (1)$$

Here s is a dimensionless "reaction coordinate" varied from $s = 0$ to 1. x^{DBA} and x^{VA} represent the equilibrium structures of the diffuse dipole-bound state ($s = 0$) and the valence anion state ($s = 1$), respectively. This scheme is exactly the same as that employed by Sommerfeld.[28,43−45] All electronic structure calculations presented in this work were performed with the GAUSSIAN-03 code.[52] Figure 1 displays one-dimensional potential energy profiles of U^- obtained from the five DFT levels along with the electron propagator based ADC result of Sommerfeld.[28] Notice that the zero energy level is taken to be the energy of the dipole-bound anion state minimum ($s = 0$). The ADC result of Sommerfeld shows that the dipole-bound and valence anion states are nearly isoenergetic; however, he mentioned that the ADC level is roughly comparable with MP2 level results.[28] For the energy difference between the dipole-bound and valence anion states (without zero-point energy correction), the most recent and more accurate value is reported to be 133 meV, which has been obtained from large-scale ab initio wave function-based calculations combined with the basis set extrapolation scheme by Bachorz et al.[36] Interestingly, the DFT calculation with the BH&HLYP functionals is found to give a very encouraging result of 160 meV. On the other hand, it is seen that the B3LYP, B3PW91, and X3LYP methods give very different results; the valence anion state is always more stable than the dipole-bound state. We can see that the dipole-bound state obtained at the B3LYP, B3PW91, or X3LYP level is not a minimum on the anion potential energy surface. This result is consistent with previous B3LYP studies of Li et al.[26] and comes from the fact that the B3LYP method significantly

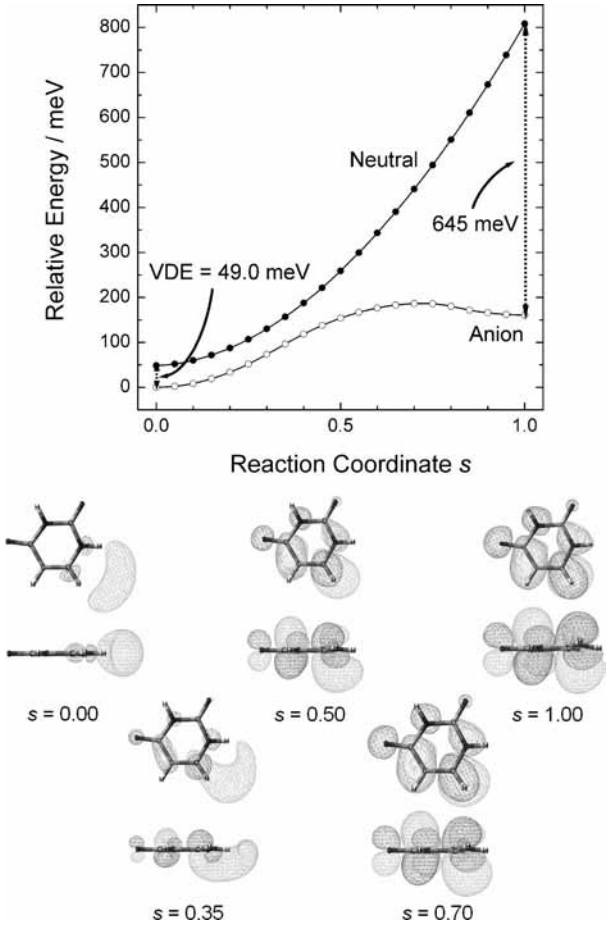

Figure 2. Potential energy profiles of neutral and anionic uracil along the linear scaling factor *s* calculated at the BH&HLYP level of theory. Singly occupied orbitals at some selected points are shown. All orbitals use the same isosurface value of 0.02 au.

overestimates the stability of the π^* valence anion state. It is important to mention recent DFT studies on water cluster anions by Herbert and Head Gordon.[53,54] They have calculated vertical detachment energies (VDEs) for various conformers of $(H_2O)_n^-$ using both wave function-based electronic structure methods and some DFT methods. Although the $(H_2O)_n^-$ clusters have only dipole-bound anion states unlike the uracil anion case, they found that the BH&HLYP level calculations give comparable results to very accurate CCSD(T) results. Also, common exchange-correlation functionals such as BLYP and B3LYP significantly overestimate the VDE values for the $(H_2O)_n^-$ clusters.

Figure 2 displays the potential energy curves for both neutral and anionic uracil along the dimensionless coordinate *s* obtained from the BH&HLYP level calculation. Also shown in this figure are singly occupied molecular orbitals of U^- at some selected points. All the orbitals in Figure 2 are drawn at the same isosurface value of 0.02 au. This means that the orbital for the dipole-bound state would be more diffuse than that for the valence anion state if we plot the orbitals based on electron density.[55] Thus, the electron density within the plotted orbital gradually increases from $s = 0$ to 1. Nevertheless, it is seen that an extra electron is smoothly transferred from the diffuse orbital to the π^* antibonding orbital with an increase of *s*. The VDE value for the dipole-bound state and valence anion state were calculated to be 49 and 647 meV, respectively. The former value is somewhat smaller than the highly accurate value (71 meV) of Bachroz et al.[30,36] This is simply because our calculations do not include too diffuse basis functions. To confirm this, we have carried out additional single-point calculations using diffuse basis functions up to 6s6p on H atoms with the same scaling factor. The obtained VDE values for the dipole-bound anion state ($s = 0$) were 74, 102, 123, and 125 meV for +3s3p, +4s4p, +5s5p, and +6s6p basis functions. This result indicates that very diffuse functions are necessary to obtain fully converged VDE values. On the other hand, the VDE value at the valence anion minimum ($s = 1$) is somewhat larger than that of the accurate value (596 meV) of Bachroz et al.[36] From Figure 2 the transition state behavior is clearly seen at $s = 0.7$. Using the geometry at this point as an initial geometry, we have carried out transition state geometry optimization at the BH&HLYP level of theory. The obtained transition state structure is presented in Figure 3 along with atomic displacement vectors for the imaginary frequency mode. We can see that this vibrational mode nearly corresponds to the out-of-plane bending motion (approximately a″-mode) of the hydrogen atom at the C_6 position. This is quite reasonable since the singly occupied orbital has a π^* character for the C_5-C_6 bond. We notice that the motion of the H atom at the N_1 position also has a small contribution to the displacement vectors. The barrier height measured from the dipole-bound minimum was calculated to be 178 meV, while the barrier height measured from the π^* valence anion minimum is only 17 meV without zero-point vibrational energy corrections. Thus, the π^* valence anion minimum is located in a very shallow well at least on the BH&HLYP-level potential energy surface.

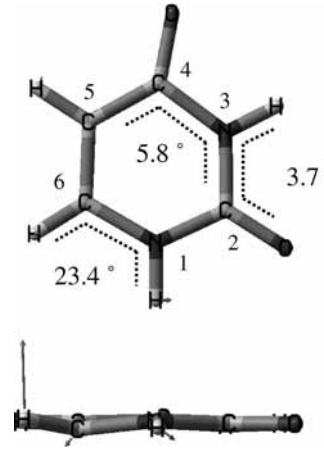

Figure 3. Optimized transition state structure between the dipole-bound and π^* valence anion states. Arrows indicate atomic displacement vectors of the imaginary frequency mode ($\nu^{\ddagger} = 1210\ cm^{-1}$).

Next we have constructed a two-dimensional potential energy surface as a function of the out-of-plane angle of H at the C_6 position and the N_1-H distance corresponding to the dissociation coordinate to form $(U-H)^- + H$. Other internal coordinates were optimized with respect to the energy. The resulting contour plot is presented in Figure 4. Needless to say, the out-of-plane bending of H at the C_6 position plays the most important role in transformation between the dipole-bound anion and π^* valence anion. It is also interesting to notice that a weak crossing seam passing through the saddle point is seen. Thus, the obtained potential energy profile is a result of electronic coupling between the dipole-bound and valence anion states of uracil, as was previously pointed out by Sommerfeld.[28] The present result strongly suggests that transformation between the dipole-bound anion and π^* valence anion can easily occur when a sufficient energy is partitioned into the C_6-H out-of-place vibrational motion via electron collisions. We have also calculated a two-

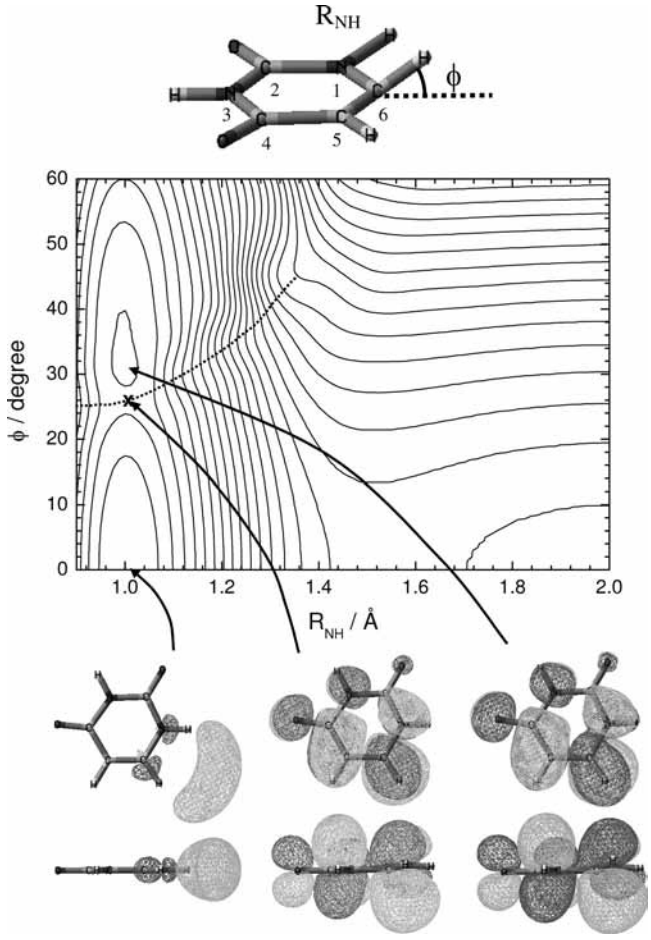

Figure 4. Contour plot of the two-dimensional potential energy surface as a function of the C_6-H out-of-plane angle (ϕ) and the N_1-H internuclear distance (R_{NH}) calculated at the BH&HLYP level. The cross indicates the saddle point and dotted line corresponds to the crossing seam. Singly occupied orbitals at the two minima and the saddle point are also shown with the same isosurface value of 0.02 au. The contour increment is 2 kcal/mol and the zero energy is defined as the dipole-bound anion minimum.

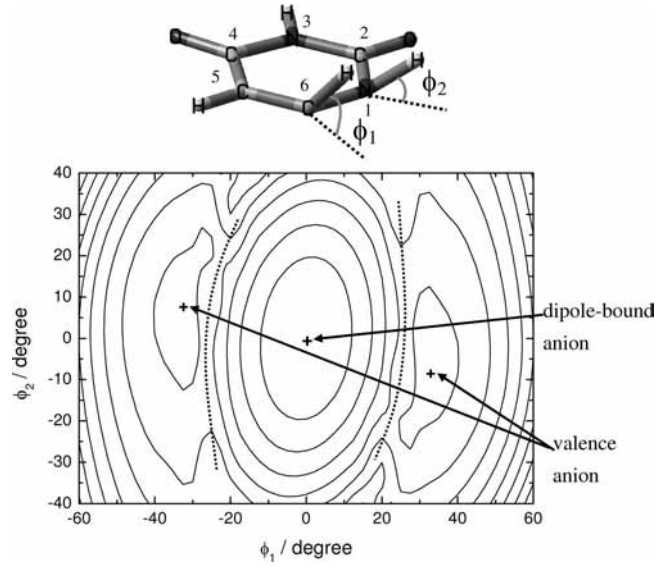

Figure 5. Contour plot of the two-dimensional potential energy surface as a function of the C_6-H (ϕ_1) and N_1-H (ϕ_2) out-of-plane angles. Crosses indicate potential minima and dotted lines correspond to crossing seams. The contour increment is 1 kcal/mol and the zero energy is defined as the dipole-bound anion minimum.

dimensional potential energy surface as a function of the two out-of-place bending motions of hydrogen atoms at N_1 and C_6 positions. Other internal coordinates were fully optimized with respect to the energy similar to Figure 4. The result is presented in Figure 5, which shows a weak correlation of these two vibrational modes.

It should be emphasized that the present DFT calculation gives only the lowest electronically adiabatic potential energy surface. Unfortunately, we failed to obtain a reliable excited state potential energy surface with the time-dependent linear-response formalism. Sommerfeld[28] has estimated the coupling strength between the two different anion states by calculating both the ground state and excited state potential energy surfaces at the ADC level. A simple diabatization scheme yielded the coupling strength of about 43 meV for the uracil anion system. This small coupling suggests that the electronically adiabatic picture does not always work well for understanding this electronic isomerization dynamics. This may be an important issue that should be addressed in the near future.

Before closing this section, it is important to comment briefly on recent experimental studies of valence anions. Very recently, Bowen's group[56,57] has succeeded in detecting valence anions of DNA/RNA base molecules with exceptionally large VDE values using a very different anion source from their previous studies. For example, in the case of uracil, the photoelectron spectrum shows a broad peak with a maximum at 2.49 eV, which is much larger than that of the π^* valence anion obtained in this section (canonical tautomer configuration). On the basis of large-scale ab initio electronic structure calculations, the observed anions were assigned to other tautomers, where a hydrogen atom is transferred to another site; however, it has been pointed out that such a tautomer with a large VDE value is not the most stable species. Thus, the formation mechanism of those valence anions has not been fully understood yet.

3. Vibrational Resonance Structure on the Two-Dimensional Potential Energy Surface

To understand the vibrational resonance structure experimentally observed in the cross section for the $e^- + U \rightarrow (U-H)^- + H$ process, we have constructed a two-dimensional potential energy surface as a function of the out-of-plane motion of the hydrogen atom attached to the N_1 position and the N_1-H stretching coordinate at the BH&HLYP level of theory. We have chosen this out-of-plane motion since this a″-type mode slightly couples the dipole-bound anion state with the valence π^* anion state by deforming the uracil ring (see also Figure 3). Also, it is expected that this mode may play a role in the N_1-H dissociation dynamics since the corresponding vibrational frequency significantly decreases with the N_1-H bond increase. As mentioned before, the C_6-H out-of-plane vibration should also play an important role in the dissociation dynamics. However, since the construction of a three-dimensional potential energy surface is time-consuming, we ignored this vibration in the present preliminary dynamics calculations.

The calculated contour plot is displayed in Figure 6. Similar to Figures 4 and 5, other internal coordinates were fully optimized with respect to the energy. It is seen that the obtained potential energy surface shows an expected behavior; a barrier within C_s symmetry constraint is seen at (R_{NH}, ϕ) = (1.325 Å, 0°). Notice that this is the second-order saddle point on the potential energy surface. It is interesting to note that the bent dissociation barrier at (R_{NH}, ϕ) = (1.40 Å, ±48.0°) measured from the dipole-bound anion potential minimum (1.00 Å, 0°)

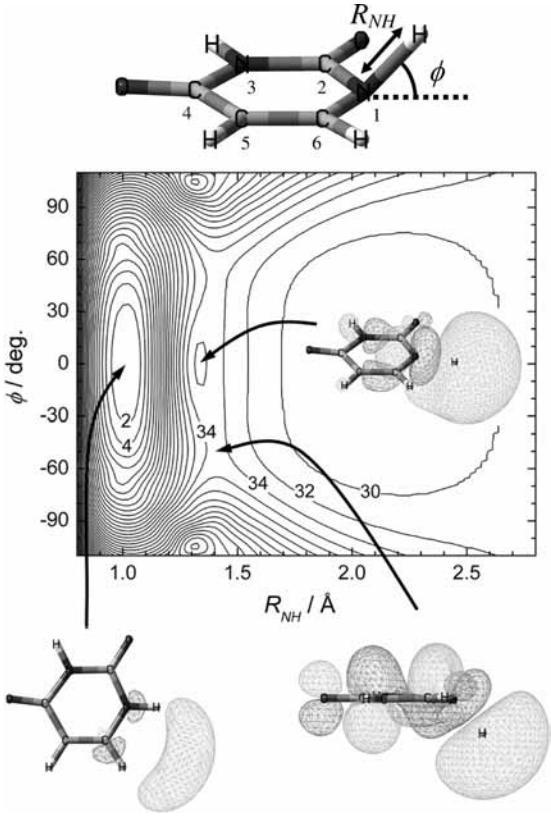

Figure 6. Contour plot of the two-dimensional potential energy surface as a function of the N_1-H out-of-plane angle (ϕ) and the N_1-H internuclear distance (R_{NH}) calculated at the BH&HLYP level. The contour increment is 2 kcal/mol and the zero energy is defined as the dipole-bound anion minimum. Singly occupied orbitals at stationary points are also shown with the same isosurface value of 0.02 au.

is somewhat smaller than that at (1.325 Å, 0°). This is because the origin of this barrier comes from the avoided crossing between the repulsive σ^* state and the N_1-H bonding state; i.e., the σ^* state potential at $\phi = 0°$ is slightly more repulsive than that at $\phi = \pm 48°$. Singly occupied molecular orbitals at stationary points are also displayed in Figure 6. We can see that the diffuse dipole-bound orbital mixes with the N_1-H σ^* orbital at the C_s saddle point. On the other hand, the valence π^* orbital strongly mixes with the N_1-H σ^* orbital at the bent saddle points. This behavior clearly implies that the π^* valence anion state can play an important role in the N_1-H dissociation dynamics.

It can be seen that there is a shallow potential well around $R_{NH} \sim 2$ Å in Figure 6. Previous theoretical studies at the B3LYP level by Li et al.[26,27] also report shallow wells along both the N_1-H and N_3-H stretch coordinates. Those potential wells are presumably due to charge-induced-type attractive interaction between $(U-H)^-$ and H. Interestingly, such a potential well was not observed along the C−H stretching coordinate. This is because negative charge is nearly localized on the N_1 or N_3 atom in the $(U-H)^-$ anion, where the H atom is dissociated from the N site, due to larger electron affinities at the N site. On the other hand, negative charge is somewhat delocalized in the $(U-H)^-$ anion where H is dissociated from the C site. It should be mentioned that the one-dimensional potential energy curve of Scheer et al.[29] does not have a shallow potential well and is purely repulsive for $R_{NH} > 1.5$ Å.

We have to point out that the potential energy surface calculated at the BH&HLYP level of theory gives an inaccurate dissociation limit. The BH&HLYP calculation gives the energy difference between the neutral equilibrium U and the $(U-H)^- + H$ dissociation limit to be 0.95 and 1.33 eV with and without zero-point energy correction, respectively. These values are much larger than the experimental appearance energy of the $(U-H)^- + H$ production channel (~0.6 eV)[14] although the accurate dissociation energy cannot be determined directly from electron−molecule scattering experiments. The present result is also in contrast with the previous B3LYP study of Li et al.,[26,27] where fairly accurate dissociation limits were obtained. Therefore, we have applied the following Gaussian scaling factor so that the calculated potential energy surface gives a reasonable dissociation limit as

$$f(R_{N_1H}) = \alpha \exp[-\beta(R_{N_1H} - R^e_{N_1H})^2] + 1 - \alpha \quad (R_{N_1H} > R^e_{N_1H}) \tag{2}$$

Here α and β are adjustable parameters and $R^e_{N_1H}$ is the equilibrium N_1-H distance (1.003 Å) at the dipole-bound anion. We employed the following values, $\alpha = 0.33$ Å^{-2} and $\beta = 35$ Å^{-2}. These values yielded the dissociation limit to be 21.2 kcal/mol (see Figure 7a below).

With the two-dimensional potential energy surface thus modified, we have carried out time-dependent wave packet calculations to obtain the state density profile above the $(U-H)^- + H$ dissociation threshold energy. The initial wave packet was constructed from the two-dimensional neutral state potential energy surface and the time-evolution of the wave packet was calculated by using the standard split-operator method on the two-dimensional grid points. In actual calculations, we employed Cartesian coordinates with $x = R_{N_1H} \cos \phi$ and $y = R_{N_1H} \sin \phi$ and the corresponding kinetic energies were evaluated by using the standard fast-Fourier-transform algorithm. To avoid unphysical reflection of the wave packet at the edge of the grid, numerically optimized complex linear-type absorbing potentials were used. The state density spectrum was extracted from the Fourier transform of the autocorrelation function.

Figure 7b displays the calculated state density spectrum. Needless to say, one cannot compare the calculated spectrum directly to the experimentally measured cross sections since our calculations do not include electron capture processes. However, we believe that the present reduced-dimensionality calculation can provide a qualitative picture of vibrational resonance structures. From the result presented in Figure 7b, it is clearly seen that the system has several resonance states above the $(U-H)^- + H$ dissociation threshold despite only two degrees-of-freedom being taken into account in the present dynamics. The state density presented in Figure 7b shows an expected behavior; relatively sharp resonance peaks can be seen in the energy range just above the $(U-H)^- + H$ dissociation threshold but below the dissociation barrier at $R_{N_1H} \approx 1.4$ Å. We found that most of these resonances correspond to the vibrational states with the vibrational quantum numbers being ($v_1 = 0$ or 1, v_2), where v_1 is the vibrational quantum number of the N_1-H stretching while v_2 is the quantum number of the out-of-plane bending. We found that the quantum number v_2 is generally quite large ($v_2 \gg 0$) for those resonance states. The energy widths for these resonances were estimated to be relatively small in the range of about 0.01−0.05 kcal/mol. The wave function density of one of these resonance states is displayed in Figure 7c as a function of (x, y) Cartesian coordinates. On the contrary, somewhat broad resonance peaks can be seen just above the dissociation barrier at $R_{N_1H} \approx 1.4$ Å. The corresponding energy width is about 0.5 kcal/mol. The wave function densities for these resonances are also presented in Figure 7c. Notice that

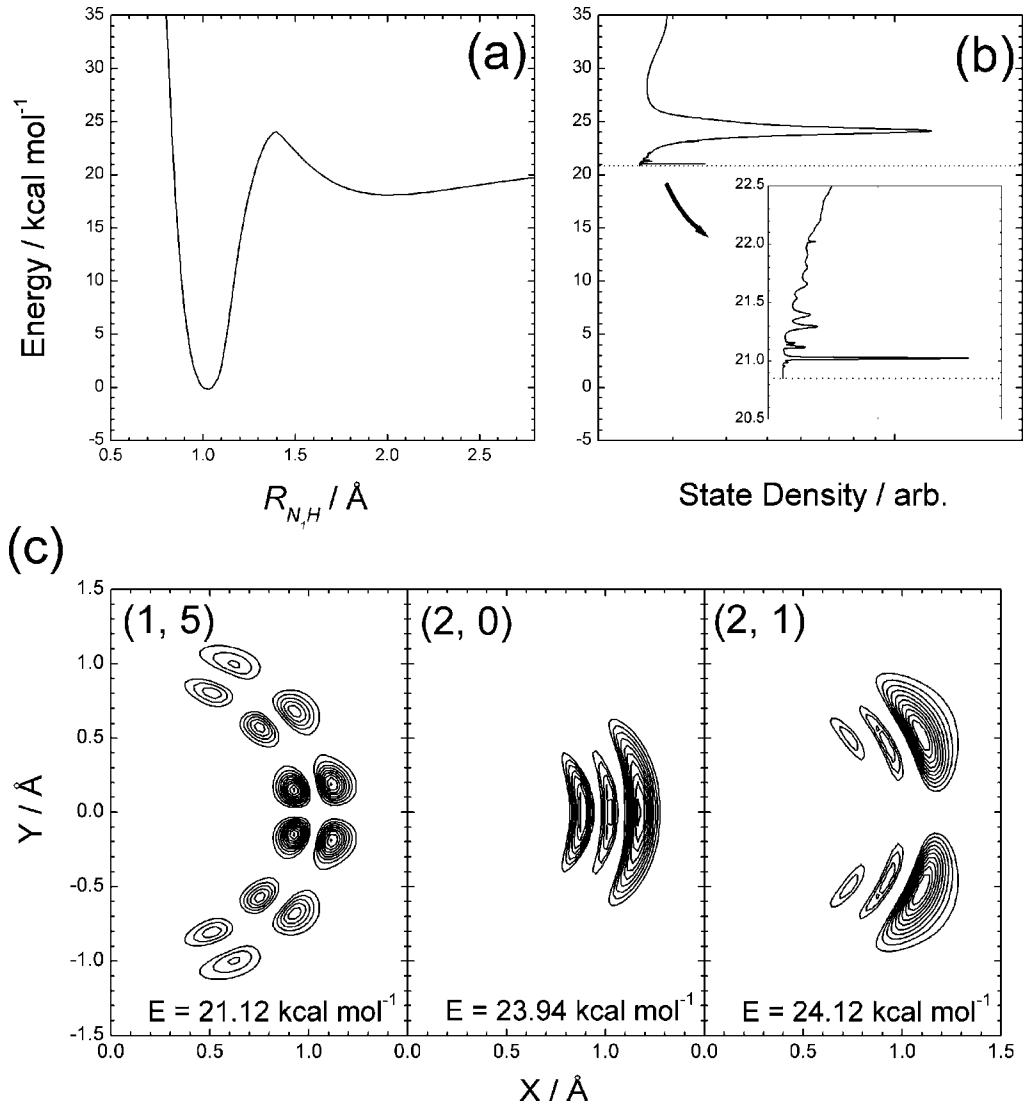

Figure 7. (a) One-dimensional cut of the potential energy surface along the N_1-H internuclear distance. (b) State density profile calculated from two-dimensional wave-packet calculations. (c) Wave function densities for selected resonance positions as a function of (x, y) Cartesian coordinates (see text).

these resonances correspond to the $v_1 = 2$ states with v_2 being 0 or 1. Unfortunately, we could not find the $v_1 = 3$ resonance state although Scheer et al.[29] have found the $v_1 = 3$ resonance state just below the dissociation barrier in their one-dimensional calculation. It should be emphasized that the resonance pattern is generally quite sensitive to subtle features of the potential energy surface employed. In particular, it is easily expected that the dissociation barrier height may play the most important role in the present case. More accurate potential energy values are definitely necessary for more quantitative discussion. Also, it may be important to understand the effect of other vibrational degrees of freedom on resonance patterns. Nevertheless, we believe that the present theoretical study would be a good starting point for further quantitative understanding of resonance structures in the dissociative electron attachment process of uracil and other DNA/RNA base molecules.

4. Summary and Future Work

In this work we have investigated the lowest electronically adiabatic potential energy surface of the uracil radical anion, where an excess electron is bound to the molecule, using the standard DFT methods to understand the mechanism of the dissociative electron attachment process, $e^- + U \rightarrow U^{-*} \rightarrow (U-H)^- + H$. It was found that the BH&HLYP level calculation give a reasonable behavior, which can describe both the diffuse dipole-bound anion state and the valence anion state in a balanced way. Similar to previous DFT studies, common exchange-correlation functionals such as B3LYP cannot describe the dipole-bound anion state and significantly overestimate the stability of the π^* valence anion state. The transition state structure between the electronic isomerization between the dipole-bound anion and π^* valence anion was successfully optimized at the BH&HLYP level and it was found that the a″-type out-of-plane motion of the hydrogen atom at the C_6 position plays the most important role in the electronic isomerization pathway between the dipole-bound and valence anion states. We have then calculated two-dimensional potential energy surfaces as a function of appropriate internal coordinates. We have shown that the π^* valence anion state plays a role in the N_1-H dissociation dynamics for the uracil anion.

We have also performed time-dependent quantum wave packet calculations by taking only two active motions, the N_1-H stretching and the out-of-plane bending of H at the N_1 site, into the dynamics to obtain the information on vibrational resonance

structures above the $(U-H)^- + H$ dissociation threshold energy. We found several resonance states although we had to apply a scaling factor so that the calculated potential energy surface gives a reasonable dissociation limit. More accurate electronic structure calculations that yield accurate dissociation limit should be definitely performed to obtain reliable vibrational resonance structures. Also, other important degrees of freedom including the C_6-H out-of-plane vibration should be taken in the future dynamics calculations. Nevertheless, we believe that the present theoretical calculations provide some important factors for understanding the dissociative electron attachment mechanisms of uracil.

Finally, it should be emphasized that further theoretical work is still needed to obtain absolute cross sections of the dissociative electron attachment process of uracil at a more quantitative level. In particular, we did not consider electron capture processes nor excess electron detachment processes at all since quantum chemistry type calculations were done in this work. Recently, elastic cross sections of electron collisions with gas-phase DNA/RNA base molecules have been calculated by using time-independent quantum electron-scattering techniques.[58−63] Although these calculations give important information on electron capture processes through electronic resonance states, they did not give any information on the dissociation dynamics since fixed-nuclei approximations are usually employed. Thus, electron-scattering methodologies including nuclear motions should be developed in the near future.

Acknowledgment. This work was supported by the Grant-in-Aid for Scientific Research of the Ministry of Education, Culture, Sports, Science, and Technology of Japan (Grant No. 20038011).

References and Notes

(1) Boudaiffa, B.; Cloutier, P.; Hunting, D.; Huels, M. A.; Sanche, L. *Science* **2000**, *287*, 1658.
(2) Sanche, L. *Eur. Phys. J. D* **2005**, *35*, 367.
(3) Simons, J. *Acc. Chem. Res.* **2006**, *39*, 772.
(4) Hanel, G.; Gstir, B.; Denifl, S.; Scheier, P.; Probst, M.; Farizon, B.; Farizon, M.; Illenberger, E.; Märk, T. D. *Phys. Rev. Lett.* **2003**, *90*, 188104.
(5) Abouaf, R.; Pommier, J.; Dunet, H. *Int. J. Mass Spectrom.* **2003**, *226*, 397.
(6) Denifl, S.; Ptasinska, S.; Cingel, M.; Matejcik, M.; Scheier, P.; Märk, T. D. *Chem. Phys. Lett.* **2003**, *377*, 74.
(7) Scheer, A. M.; Aflatooni, K.; Gallup, G. A.; Burrow, P. D. *Phys. Rev. Lett.* **2004**, *92*, 068102.
(8) Denifl, S.; Ptasińska, S.; Hanel, G.; Gstir, B.; Probst, M.; Scheier, P.; Märk, T. D. *J. Chem. Phys.* **2004**, *120*, 6557.
(9) Denifl, S.; Ptasińska, S.; Probst, M.; Hrušák, J.; Scheier, P.; Märk, T. D. *J. Phys. Chem. A* **2004**, *108*, 6562.
(10) Abouaf, R.; Dunet, H. *Eur. Phys. J. D* **2005**, *35*, 405.
(11) Ptasinska, S.; Denifl, S.; Scheier, P.; Illenberger, E.; Märk, T. D. *Angew. Chem., Int. Ed.* **2005**, *44*, 6941.
(12) Ptasińska, S.; Denifl, S.; Grill, V.; Märk, T. D.; Scheier, P.; Gohlke, S.; Huels, M. A.; Illenberger, E. *Angew. Chem., Int. Ed.* **2005**, *44*, 1647.
(13) Aflatooni, K.; Scheer, A. M.; Burrow, P. D. *Chem. Phys. Lett.* **2005**, *408*, 426.
(14) Burrow, P. D.; Gallup, G. A.; Scheer, A. M.; Denifl, S.; Ptasinska, S.; Märk, T.; Scheier, P. *J. Chem. Phys.* **2006**, *124*, 124310.
(15) Denifl, S.; Zappa, F.; Mähr, I.; Lecointre, J.; Probst, M.; Märk, T. D.; Scheier, P. *Phys. Rev. Lett.* **2006**, *97*, 043201.
(16) Denifl, S.; Sulzer, P.; Huber, D.; Zappa, F.; Probst, M.; Märk, T. D.; Scheier, P.; Injan, N.; Limtrakul, J.; Abouaf, R.; Dunet, H. *Angew. Chem., Int. Ed.* **2007**, *46*, 5238.
(17) Denifl, S.; Zappa, F.; Mauracher, A.; da Silva, F. F.; Bacher, A.; Echt, O.; Märk, T. D.; Bohme, D. K.; Scheier, P. *ChemPhysChem* **2008**, *9*, 1387.
(18) Oyler, N. A.; Adamowicz, L. *J. Phys. Chem.* **1993**, *97*, 11122.
(19) Desfrançois, C.; Periquet, V.; Bouteiller, Y.; Schermann, J. P. *J. Phys. Chem. A* **1998**, *102*, 1274.
(20) Dolgounitcheva, O.; Zakrzewski, V. G.; Ortiz, J. V. *Chem. Phys. Lett.* **1999**, *307*, 220.
(21) Russo, N.; Toscano, M.; Grand, A. *J. Comput. Chem.* **2000**, *14*, 1243.
(22) Wetmore, S. D.; Boyd, R. J.; Eriksson, L. A. *Chem. Phys. Lett.* **2000**, *322*, 129.
(23) Wesolowski, S. S.; Leininger, M. L.; Pentchev, P. N.; Schaefer, H. F., III *J. Am. Chem. Soc.* **2001**, *123*, 4023.
(24) Li, X.; Cai, Z.; Sevilla, M. D. *J. Phys. Chem. A* **2002**, *106*, 1596.
(25) Li, X.; Sanche, L.; Sevilla, M. D. *J. Phys. Chem. A* **2002**, *106*, 11248.
(26) Li, X.; Sanche, L.; Sevilla, M. D. *J. Phys. Chem. B* **2004**, *108*, 5472.
(27) Li, X.; Sevilla, M. D.; Sanche, L. *J. Phys. Chem. B* **2004**, *108*, 19013.
(28) Sommerfeld, T. *J. Phys. Chem. A* **2004**, *108*, 9150.
(29) Scheer, A. M.; Silvernail, C.; Belot, J. A.; Aflatooni, K.; Gallup, G. A.; Burrow, P. D. *Chem. Phys. Lett.* **2005**, *411*, 46.
(30) Bachorz, R. A.; Rak, J.; Gutowski, M. *Phys. Chem. Chem. Phys.* **2005**, *7*, 2116.
(31) Svozil, D.; Frigato, T.; Havlas, Z.; Jungwirth, P. *Phys. Chem. Chem. Phys.* **2005**, *7*, 840.
(32) Luo, Q.; Li, J.; Li, Q. S.; Kim, S.; Wheeler, S. E.; Xie, Y.; Schaefer, H. F., III *Phys. Chem. Chem. Phys.* **2005**, *7*, 861.
(33) Dąbkowska, I.; Rak, J.; Gutowski, M. *Eur. Phys. J. D* **2005**, *35*, 429.
(34) Théodore, M.; Sobczyk, M.; Simons, J. *Chem. Phys.* **2006**, *329*, 139.
(35) Kumar, A.; Sevilla, M. D. *J. Phys. Chem. B* **2007**, *111*, 5464.
(36) Bachorz, R. A.; Klopper, W.; Gutowski, M. *J. Chem. Phys.* **2007**, *126*, 085101.
(37) Haranczyk, M.; Gutowski, M. *J. Am. Chem. Soc.* **2005**, *127*, 699.
(38) Dolgounitcheva, O.; Zakrzewski, V. G.; Ortiz, J. V. *J. Phys. Chem. A* **2001**, *105*, 8782.
(39) Puiatti, M.; Vera, D. M. A.; Pierini, A. B. *Phys. Chem. Chem. Phys.* **2008**, *10*, 1394.
(40) Harańczyk, M.; Rak, J.; Gutowski, M. *J. Phys. Chem. A* **2005**, *109*, 11495.
(41) Smith, D. M. A.; Jalbout, A. F.; Smets, J.; Adamowicz, L. *Chem. Phys.* **2000**, *260*, 45.
(42) Roca-Sanjuán, D.; Merchán, M.; Serrano-Andrés, L.; Rubio, M. *J. Chem. Phys.* **2008**, *129*, 095104.
(43) Sommerfeld, T. *ChemPhysChem* **2001**, *11*, 677.
(44) Sommerfeld, T. *Phys. Chem. Chem. Phys.* **2002**, *4*, 2511.
(45) Sommerfeld, T. *J. Phys. Conf. Ser.* **2005**, *4*, 245.
(46) Becke, A. D. *J. Chem. Phys.* **1993**, *98*, 5648.
(47) Lee, C.; Yang, W.; Parr, R. G. *Phys. Rev. B* **1988**, *37*, 785.
(48) Becke, A. D. *J. Chem. Phys.* **1993**, *98*, 1372.
(49) We use BH&H and BH&HLYP implemented in Gaussian03 (ref 52): $E_{XC}^{BH\&H} = {}^1/_2E_X^{HF} + {}^1/_2E_X^{Slater} + E_C^{LYP}$ and $E_{XC}^{BH\&HLYP} = {}^1/_2E_X^{HF} + {}^1/_2E_X^{B88} + E_C^{LYP}$.
(50) Perdew, J. P.; Burke, K.; Wang, Y. *Phys. Rev. B* **1996**, *54*, 16533.
(51) Xu, X.; Goddard, W. A., III *Proc. Natl. Acad. Sci. U. S. A.* **2004**, *101*, 2673.
(52) Frisch, M. J. , *Gaussian03*, Revision D.02; Gaussian, Inc., Pittsburgh, PA, 2004.
(53) Herbert, J. M.; Head-Gordon, M. *J. Phys. Chem. A* **2005**, *109*, 5217.
(54) Herbert, J. M.; Head-Gordon, M. *Phys. Chem. Chem. Phys.* **2006**, *8*, 68.
(55) Haranczyk, M.; Gutowski, M. *J. Chem. Theory Comput.* **2008**, *4*, 689.
(56) Li, X.; Bowen, K. H.; Haranczyk, M.; Bachorz, R. A.; Mazurkiewicz, K.; Rak, J.; Gutowski, M. *J. Chem. Phys.* **2007**, *127*, 174309.
(57) Bachorz, R. A.; Klopper, W.; Gutowski, M.; Li, X.; Bowen, K. H. *J. Chem. Phys.* **2008**, *129*, 054309.
(58) Gianturco, F. A.; Lucchese, R. R. *J. Chem. Phys.* **2004**, *120*, 7446.
(59) Gianturco, F. A.; Sebastianelli, F.; Lucchese, R. R.; Baccarelli, I.; Sanna, N. *J. Chem. Phys.* **2008**, *128*, 174302.
(60) Tonzani, S.; Greene, C. H. *J. Chem. Phys.* **2006**, *124*, 054312.
(61) Winstead, C.; McKoy, V. *J. Chem. Phys.* **2006**, *125*, 174304.
(62) Winstead, C.; McKoy, V. *J. Chem. Phys.* **2006**, *125*, 244302.
(63) Winstead, C.; McKoy, V.; d'Almeida Sanchez, S. *J. Chem. Phys.* **2007**, *127*, 085105.

JP808885X